Journal of Applied Physics

# Annealing behaviors of vacancy-type defects in AlN deposited by radio-frequency sputtering and metalorganic vapor phase epitaxy studied using monoenergetic positron beams

Cite as: J. Appl. Phys. 128, 085704 (2020); https://doi.org/10.1063/5.0015225
Submitted: 26 May 2020 • Accepted: 07 August 2020 • Published Online: 28 August 2020

Akira Uedono, Kanako Shojiki, Kenjiro Uesugi, et al.

View Online

Export Citation

CrossMark

ARTICLES YOU MAY BE INTERESTED IN

Suppression of dislocation-induced spiral hillocks in MOVPE-grown AlGaN on face-to-face annealed sputter-deposited AlN template
Applied Physics Letters 116, 062101 (2020); https://doi.org/10.1063/1.5141825

AlGaN-based deep UV LEDs grown on sputtered and high temperature annealed AlN/sapphire
Applied Physics Letters 112, 041110 (2018); https://doi.org/10.1063/1.5010265

Impact of face-to-face annealed sputtered AlN on the optical properties of AlGaN multiple quantum wells
AIP Advances 9, 125342 (2019); https://doi.org/10.1063/1.5125799

Lock-in Amplifiers
up to 600 MHz

© 2020 Author(s).

Journal of Applied Physics | ARTICLE | scitation.org/journal/jap

# Annealing behaviors of vacancy-type defects in AlN deposited by radio-frequency sputtering and metalorganic vapor phase epitaxy studied using monoenergetic positron beams

Cite as: J. Appl. Phys. **128**, 085704 (2020); doi: 10.1063/5.0015225
Submitted: 26 May 2020 · Accepted: 7 August 2020 ·
Published Online: 28 August 2020

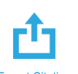

Akira Uedono,[1,a)] Kanako Shojiki,[2] Kenjiro Uesugi,[3] Shigefusa F. Chichibu,[4] Shoji Ishibashi,[5] Marcel Dickmann,[6] Werner Egger,[6] Christoph Hugenschmidt,[7] and Hideto Miyake[2,8]

## AFFILIATIONS

[1]Division of Applied Physics, Faculty of Pure and Applied Science, University of Tsukuba, Tsukuba, Ibaraki 305-8573, Japan
[2]Graduate School of Engineering, Mie University, 1577 Kurimamachiya, Tsu, Mie 514-8507, Japan
[3]Strategic Planning Office for Regional Revitalization, Mie University, 1577 Kurimamachiya, Tsu, Mie 514-8507, Japan
[4]Institute of Multidisciplinary Research for Advanced Materials, Tohoku University, Sendai 980-8577, Japan
[5]Research Center for Computational Design of Advanced Functional Materials (CD-FMat), National Institute of Advanced Industrial Science and Technology (AIST), Tsukuba, Ibaraki 305-8568, Japan
[6]Universität der Bundeswehr München, Institut für Angewandte Physik und Messtechnik, 85577 Neubiberg, Germany
[7]Physics Department E21 and Heinz Maier-Leibnitz Zentrum (MLZ), Technische Universität München, 85748 Garching, Germany
[8]Graduate School of Regional Innovation Studies, Mie University, 1577 Kurimamachiya, Tsu, Mie 514-8507, Japan

[a)]**Author to whom correspondence should be addressed:** uedono.akira.gb@u.tsukuba.ac.jp

## ABSTRACT

Vacancy-type defects in AlN films were probed by using monoenergetic positron beams. The AlN films were deposited on sapphire substrates by using a radio-frequency sputtering technique. Epitaxial films grown by metalorganic vapor phase epitaxy on the sputtered AlN films were also characterized. For the sputtered AlN, the major defect species was identified to be complexes between Al-vacancy and oxygen atoms located at nitrogen sites. Vacancy clusters were introduced after annealing at 1300 °C in the $N_2$ atmosphere but their concentration decreased with a higher annealing temperature. The vacancy–oxygen complexes, however, still existed in the AlN film after annealing at 1700 °C. For the AlN epitaxial films, the concentration of vacancy clusters increased as the growth temperature increased up to 1300 °C but it decreased with the post-growth annealing at 1700 °C.

*Published under license by AIP Publishing.* https://doi.org/10.1063/5.0015225

## I. INTRODUCTION

AlGaN has attracted intense research interest due to its unique properties and potential applications in short-wavelength light-emitting diodes (LEDs) and laser diodes (LDs).[1–4] The ability of GaN to form solid solutions with AlN, making bandgap engineering possible (3.4–6.0 eV), is essential for defining the emission wavelength of the LEDs and LDs that cover almost the entire ultraviolet (UV) range (210–370 nm). The major applications of UV-LEDs and LDs are water purification, UV curing/printing, environmental/medical sensing, plant growth lighting, phototherapy, etc.[2,4] Various gases or solid-state UV lasers and mercury lamps have been used for such UV applications but their bulky/fragile nature and high heat generation restrict their design and application. With excellent properties including compactness, low operating power, and long lifetime, UV-LEDs and UV-LDs are ready to replace them and are expected to open new applications of UV light.

To date, most AlN and AlGaN layers have been heteroepitaxially grown on sapphire substrates by using metalorganic vapor


Published under license by AIP Publishing.

phase epitaxy (MOVPE), halide vapor phase epitaxy, sputtering, etc.[1–10] Because of the lattice mismatch and difference in coefficients of thermal expansion between sapphire and AlGaN, the major defects in AlGaN films are known to be threading dislocations, where the typical dislocation density is reported to be in the order of $10^9$–$10^{10}$ $cm^{-2}$. Because the dislocations act as non-radiative recombination channels, they are the main cause of the reduction in external quantum efficiencies of devices.[11] Decreasing the threading dislocation density (TDD) in AlGaN, therefore, is one of the key issues to overcome in order to obtain highly efficient UV optoelectronic devices. Recently, Uesugi et al.[12] reported that the thick AlN film with a low TDD ($2 \times 10^8$ $cm^{-2}$) can be obtained through homoepitaxial growth using AlN/sapphire templates, where the templates were prepared with a combination of sputter deposition of AlN films on sapphire substrates and subsequent high-temperature annealing.[10] In this process, the major driving force of the reduction of TDD was attributed to rearrangements of atoms and a resultant strain relaxation of the sputtered AlN film during high-temperature annealing.[8–10] Thus, knowledge of the behaviors of point defects in AlN is important for controlling the quality of AlGaN and AlN deposited on a substrate.

The formation energies of self-interstitials and antisites are high in AlN, and only vacancies are supposed to have low enough formation energies to occur in high enough concentrations to affect electronic and optical properties.[11] Thus, vacancies and their complexes with impurities such as oxygen or carbon are the major concern in studying point defects in AlN. It is well known that not only extended defects but also point defects, impurities, and their complexes act as non-radiative recombination centers in AlN and AlGaN.[4,11–18] Thus, studying vacancy-type defects in AlN is important for enhancing the performance of UV-LEDs and LDs. Positron annihilation is a useful technique for characterizing vacancy-type defects in semiconductors,[19,20] and this technique has been successfully used to detect vacancy-type defects in group-III nitrides.[21–28] In the present study, we used monoenergetic positron beams to study the annealing behaviors of vacancy-type defects in AlN films grown by using a radio-frequency (RF) sputtering technique and MOVPE.

## II. EXPERIMENT

### A. Sample preparation

AlN films were grown on c-plane 2-in.-sapphire substrates with a nominal surface off-cut angle of 0.2° with respect to the *m*-axis using RF sputtering. Details on the deposition method and the properties of the films prepared using this method are given elsewhere.[12,29] Polycrystalline AlN was used as a target. $N_2$ was used as the sputtering gas. The RF power and growth temperature were 700 W and 600 °C, respectively. To investigate the effect of annealing temperature, 480-nm-thick sputtered AlN films were prepared. The background pressure during the sputtering was 0.05 Pa at the $N_2$ flow rate of 24 sccm to prevent the crack formation during annealing.[12] The sputtered AlN films were annealed in $N_2$ atmosphere at 1100–1700 °C for 3 h. To suppress the thermal decomposition of AlN, the surface of the AlN films was covered with another AlN template using a "face-to-face" setup. Hereafter, these samples are referred to as "FFA Sp-AlN."

As a template for the MOVPE growth, the 180-nm-thick FFA Sp-AlN films were deposited at 0.2 Pa with Ar and $N_2$ flow rates of 18 and 72 sccm. The sputtered AlN films were face-to-face annealed at 1700 °C for 3 h. 820 nm-thick AlN films were grown using MOVPE on the FFA Sp-AlN, where the templates were annealed at 1700 °C before the growth. For the MOVPE growth of AlN (MOVPE-AlN), trimethylaluminum (TMA) and $NH_3$ (1 slm) were used as precursors, and $H_2$ (74 slm) was used as the carrier gas. The V/III ratio and the pressure of the reactor during the growth were 211 and 13 kPa, respectively. The growth temperature was varied from 1100 °C to 1340 °C.

For the AlN films, x-ray diffraction was measured using an asymmetric Ge(220) monochromator with Cu Kα1. The surface morphology was characterized by atomic force microscopy (AFM). The impurity concentration of the AlN films was measured by secondary ion mass spectroscopy (SIMS). For the FFA Sp-AlN, the major impurities were oxygen ($[O] = 6 \times 10^{20}$ $cm^{-3}$), hydrogen ($[H] = 3 \times 10^{19}$ $cm^{-3}$), carbon ($[C] = 3 \times 10^{18}$ $cm^{-3}$), and Si ($[Si] = 2 \times 10^{18}$ $cm^{-3}$) before annealing treatment. After annealing at 1700 °C, no large change in their impurity concentrations was observed except for hydrogen, where [H] decreased to the background level of the measurement ($\leq 6 \times 10^{16}$ $cm^{-3}$). In the present study, the MOVPE-AlN films were prepared by two different reactors. For the AlN films grown with different growth temperatures (1100–1340 °C), the SIMS measurements were performed for the AlN film grown at 1300 °C. Then, [O], [C], and [Si] were determined to be $1–3 \times 10^{17}$ $cm^{-3}$, $1–2 \times 10^{16}$ $cm^{-3}$, and $1 \times 10^{17}$ $cm^{-3}$, respectively. With another reactor, for the AlN film grown at 1300 °C, although [O] was the same as that for the above samples, [C] was below the detection limit ($1.5 \times 10^{16}$ $cm^{-3}$), and [Si] was $1.5 \times 10^{16}$ $cm^{-3}$. Hereafter, this sample is referred to as "reference" because the concentration of vacancy-type defects was found to be lower than that for the other MOVPE-AlN films.

### B. Positron annihilation (experiments and calculations)

Details on the positron annihilation technique are given elsewhere.[19,20,30] The Doppler broadening spectra of the annihilation radiation were measured with Ge detectors as a function of the incident positron energy *E*. The measured spectra were characterized by the *S* parameter, defined as the fraction of annihilation events over the energy range of 510.22–511.78 keV, and by the *W* parameter, defined as the number of annihilation events in the energy ranges of 504.14–507.96 keV and 514.04–517.86 keV. The energy resolution of the Ge detectors was 1.2 keV (full-width at half-maximum, FWHM). Doppler broadening profiles were also measured with a coincidence system.[19] The relationship between *S* and *E* was analyzed by VEPFIT, a computer program developed by van Veen *et al.*[31] The positron lifetime spectrum was measured using a pulsed monoenergetic positron beam at the NEPOMUC positron source of the Technische Universität München.[32,33] Approximately, $4 \times 10^6$ counts were accumulated for a lifetime spectrum. The spectrum $S_{LT}(t)$ is given by $S_{LT}(t) = \sum \lambda_i I_i \exp(-\lambda_i t)$, where $\lambda_i$ and $I_i$ are the annihilation rate and intensity of positrons of the *i*th component, respectively ($\Sigma I_i = 1$). The positron lifetime $\tau_i$ is given by $1/\lambda_i$. The observed spectra were analyzed with a time resolution of 190 ps


Published under license by AIP Publishing.

(full-width at half-maximum: FWHM) using the RESOLUTION computer program.[34]

The Doppler broadening spectra and lifetime of positrons corresponding to positron annihilation in the delocalized state and trapped state in cation vacancies were calculated using QMAS (Quantum MAterials Simulator) code.[35,36] This program adopts the projector augmented-wave (PAW) method[37,38] to obtain electron wave functions. To describe the exchange and correlation energy of electrons, the generalized gradient approximation was used.[39] Details on the calculation procedure for group-III nitride semiconductors are given elsewhere.[40] For the high-frequency dielectric constant, which is used in evaluating the enhancement factor [Eq. (4) of Ref. 40], we used the experimental value of 4.7. An orthorhombic supercell equivalent to $4 \times 4 \times 2$ wurtzite cells was used for simulation and it contained 128 atoms if there are no vacancies. The supercell dimensions were $2\sqrt{3}a_0 \times 4a_0 \times 2c_0$, where $a_0 = 0.3110$ nm and $c_0 = 0.4980$ nm were the lattice parameters of the wurtzite cell. For the supercell containing a defect, atomic positions in the fixed cell (with the experimental lattice parameters) were computationally optimized through a series of first-principles electronic-structure calculations. Charge states of the defects were assumed to be neutral. Effects of the trapping of positrons on the configuration of atoms were not included in the simulation. The formalism of the local density approximation[41] was used in the calculation of the positron wave functions. Doppler broadening spectra corresponding to the annihilation of positrons in the delocalized state and the trapped states in cation vacancies were calculated. After a convolution of the simulated spectra and a Gaussian function (FWHM = 1 keV), the spectra were characterized by the $S$ and $W$ parameters (the definitions of those parameters were given above).

## III. RESULTS AND DISCUSSION

### A. Surface morphology and crystallinity of FFA Sp-AlN

Figure 1 shows AFM images for the FFA Sp-AlN films before and after annealing treatment (1300–1700 °C). For the as-deposited sample [Fig. 1(a)], tiny columnar structures covered the entire surface. As the annealing temperature increased [Figs. 1(b) and 1(c)], this structure tended to coalesce. After annealing at 1700 °C [Fig. 1(d)], a step and terrace surface morphology formed. The observed annealing behavior of the surface morphology was similar to that for the FFA Sp-AlN films reported by Xiao *et al.*[29] From measurements of AFM, XRD, and cross-sectional images obtained by scanning transmission electron microscopy (STEM), it was concluded that the columnar domains with a diameter of about 25 nm coalesced after annealing, and the domain boundaries in the FFA Sp-AlN films were almost annihilated at 1700 °C. For the samples after annealing at 1500 and 1700 °C, however, numerous hexagonal voids were observed in the STEM images, and the formation of such defects was attributed to the introduction of residual spaces due to the annihilation of the columnar structure.

Figure 2(a) shows the root mean square (RMS) roughness of the sample surface as a function of annealing temperature. The RMS value increased after 1300 °C, which can be attributed to the rearrangement of domains during annealing treatment. Figure 2(b) shows the annealing behaviors of the FWHM values of the symmetric (0002) and asymmetric $(10\bar{1}2)$ x-ray Bragg diffraction peaks of the FFA Sp-AlN films. Although the FWHM value for the (0002)-plane peak increased after annealing at 1300 °C, it kept almost constant at a higher annealing temperature. The FWHM of the $(10\bar{1}2)$-plane peak decreased as the annealing temperature increased, which can be attributed to the increase in grain size owing to the elimination of twist components and domain boundaries.[29] The value of TDD estimated from the diffraction peaks of the sample annealed at 1700 °C was $1.6 \times 10^8$ cm$^{-2}$.

### B. Detection of vacancy-type defects in FFA Sp-AlN

Figure 3 shows $S$ values as a function of the incident energy of positrons $E$ for the FFA Sp-AlN films before and after annealing (1300–1700 °C). The result for MOVPE-AlN (reference) is also shown. The mean implantation depth of positrons for the AlN film is shown on the upper horizontal axis. For the FFA Sp-AlN films, the $S$ value increased as $E$ decreased (<1 keV), which was due to the diffusion of positrons toward the surface. The $S$ values measured at $E > 25$ keV were saturated for all samples, which was due to the positron annihilation in the sapphire substrate. Flat regions in the $S$–$E$ relationships were observed at $E = 2$–$6$ keV, suggesting the annihilation of positrons in the AlN films. For the reference sample, the flat region shifted to $E = 7$–$10$ keV because the thickness of the reference sample was thicker than that for the FFA Sp-AlN films. The $S$ value for the AlN film of the reference sample was smaller than the $S$ values for the FFA Sp-AlN films, suggesting that the concentration of vacancy-type defects in the FFA Sp-AlN films was higher than that in the AlN film of the reference sample.

The solid curves in Fig. 3 are fits to the experimental data, where the data were analyzed using the sample structures described in the Sec. II B. The diffusion lengths of positrons ($L_d$) for the FFA Sp-AlN films were determined to be 4–6 nm. The typical value of $L_d$ for high-quality GaN, such as the sample grown by MOVPE or the hydride vapor phase epitaxy technique, was reported to be 60–90 nm.[30,42,43] The short diffusion length of positrons for the FFA Sp-AlN films suggests that almost all positrons annihilated from the trapped state due to the vacancy-type defects. As shown in Fig. 3, the $S$ value corresponding to the positron annihilation in the FFA Sp-AlN film increased after 1300 °C annealing, and it decreased at higher annealing temperatures. Figure 2(c) summarized the annealing behavior of $S$ calculated from the Doppler broadening spectrum obtained by the coincidence system. The measurements were done at $E = 4$ keV. Identification of the defect species will be discussed in Sec. III C.

For the reference sample, the value of $L_d$ was determined to be $36 \pm 1$ nm. As described below, the positron lifetime for this sample was close to that reported as the lifetime of positrons annihilate from the delocalized state.[27] Thus, the diffusion length of the reference sample being shorter than for defect-free AlN could be due to not only the trapping of positrons by vacancies but also the scattering of positrons by defects or impurities.

### C. Identification of vacancy-type defects in FFA Sp-AlN

When a positron annihilates in both the delocalized state and the trapped state of vacancies, the $(S,W)$ value is obtained as a


Published under license by AIP Publishing.

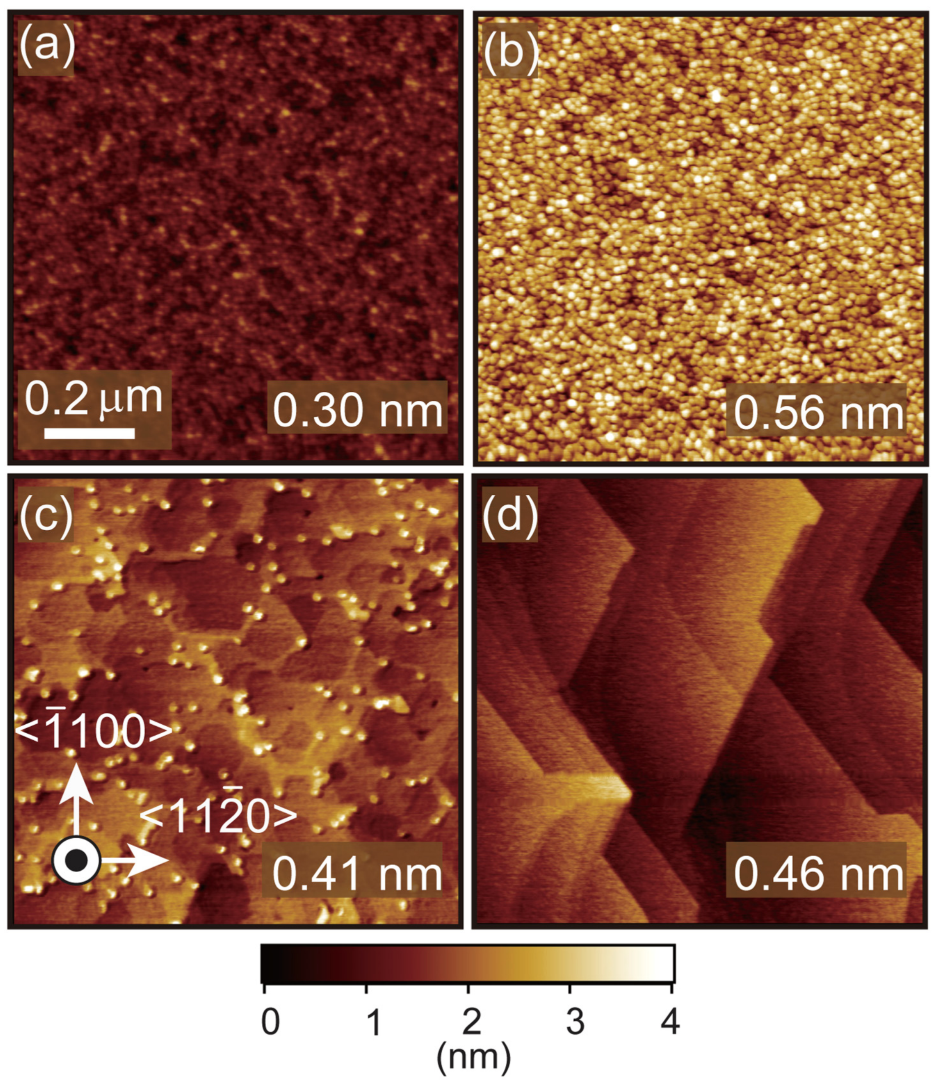


**FIG. 1.** AFM images of FFA Sp-AlN (a) before and after annealing at (b) 1300 °C, (c) 1500 °C, and (d) 1700 °C. Scanning area was 1 × 1 $\mu m^2$. RMS roughness of the sample surface is shown in the figure.

weighted average of the characteristic values for those states, and it lies on a line connecting the according values. Thus, one can discuss the defect species from the locations of measured values in the *S*–*W* plot.[19] Figure 4 shows the *S*–*W* relationships for the FFA Sp-AlN films before and after annealing (brown). These (*S*,*W*) values were obtained by the coincidence system and measured at $E = 4$ keV, where the statistical errors of the *S* and *W* values were close to the size of the symbols used in the figure. The result for the reference sample measured at $E = 8$ keV is also shown. The calculated (*S*,*W*) values for the annihilation of positrons in the delocalized state (DF), typical cation vacancies, such as the Al-vacancies ($V_{Al}$s), and their complexes with nitrogen-vacancies ($V_N$s) [$(V_{Al})_m(V_N)_n$ (m, n: integer)] are also shown in Fig. 4 (blue symbols), where the outward relaxation of nitrogen atoms surrounding $V_{Al}$ was observed. The values for complexes between $V_{Al}$ and oxygen at nitrogen sites ($O_N$) and hydrogen trapped by $V_{Al}$ [$(H)_{nAl}$, n = 1, 3, and 4] are shown in the same figure (violet symbols).

Figure 5 shows the relationship between the *S* value and the positron lifetime for (a) typical vacancy-type defects and (b) complexes between vacancies and impurities in AlN. The lifetime of positrons trapped by $V_{Al}$ was calculated to be 0.245 ns [Fig. 5(a)]. The positron lifetimes of $V_{Al}(O_N)_n$ were not that much different from that of $V_{Al}$. For $V_{Al}$-H complexes, the *S* value and positron lifetime decrease with increasing the number of hydrogen atoms trapped by $V_{Al}$.

The lifetime spectrum of positrons for the reference sample was measured at $E = 8$ keV, and it was decomposed into two components. The first and second lifetimes were $\tau_1 = 0.160 \pm 0.001$ ns and $\tau_2 = 0.353 \pm 0.005$ ns ($I_2 = 5.2 \pm 0.4\%$), respectively. Mäki *et al.*[27] reported that the positron lifetime in bulk AlN grown by the physical vapor transport (PVT) method was obtained to be 0.157–0.158 ns at


Published under license by AIP Publishing.

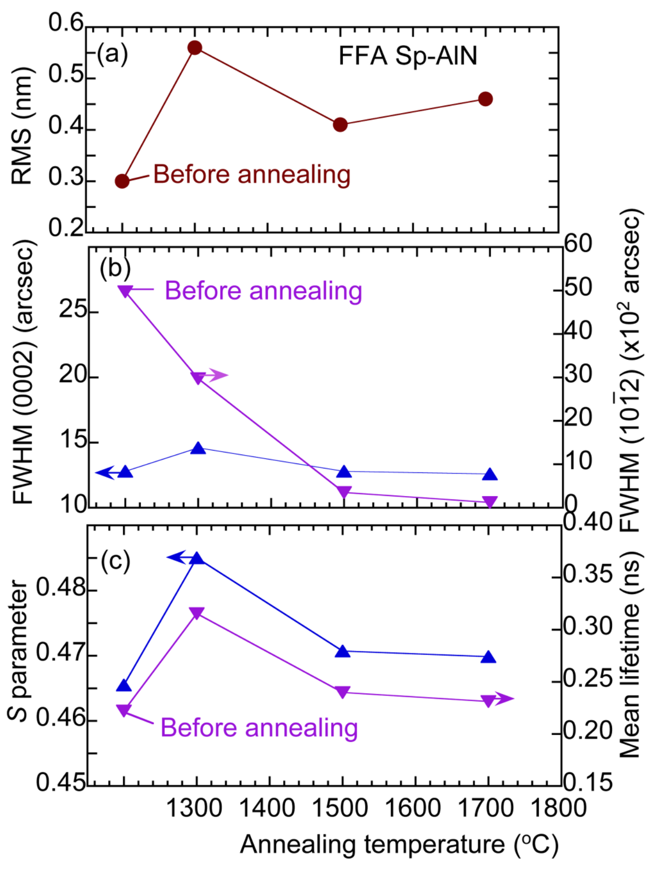


**FIG. 2.** Annealing behaviors of (a) RMS roughness of sample surface, (b) FWHM of (0002) and (10$\bar{1}$2)-plane x-ray diffraction peaks, and (c) $S$ values and mean positron lifetime ($\tau_m$) measured at $E = 4$ keV for FFA Sp-AlN.

room temperature, and this value was associated with the lifetime of positrons annihilated from the delocalized state. The first lifetime for the reference sample was close to this value. The positron lifetime for defect-free AlN was calculated to be $\tau_{df(cal)} = 0.165$ ns, which was also close to $\tau_1$. In the present work, because of the relatively long positron diffusion length, the positron annihilation at the surface affected the lifetimes and ($S$,$W$) measured at $E = 8$ keV. Thus, the second lifetime would be the lifetime of positrons at the surface. In turn, assuming that the second annihilation mode is due to the trapping of positrons by vacancy-type defects, using the two-state trapping model of positrons,[19] the calculated bulk lifetime was determined to be 0.168 ns. Because, both the first lifetime ($\tau_1 = 0.160$ ns) and the bulk lifetime calculated from the trapping model ($\tau_b = 0.168$ ns) were not that much different from the bulk lifetime reported by Mäki *et al.*[27] and $\tau_{df(cal)}$ (0.165 ns), identifying the second component for the reference sample was difficult. Because the relative intensity of the second component is not large (5%), the effect of the second component on the ($S$,$W$) value is likely to be small.

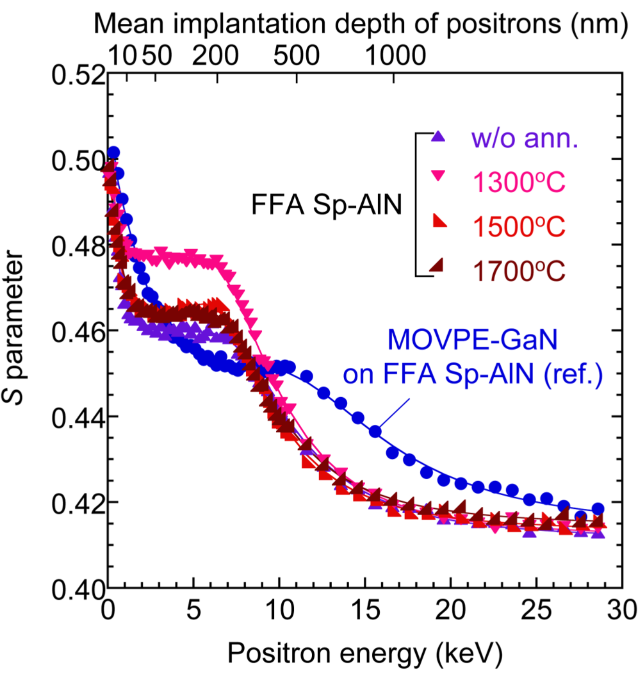


**FIG. 3.** $S$ parameter as a function of incident positron energy $E$ for FFA Sp-AlN films before and after annealing treatments at 1300–1700 °C in the $N_2$ atmosphere. The result for AlN grown on FFA Sp-AlN by MOVPE is also shown.

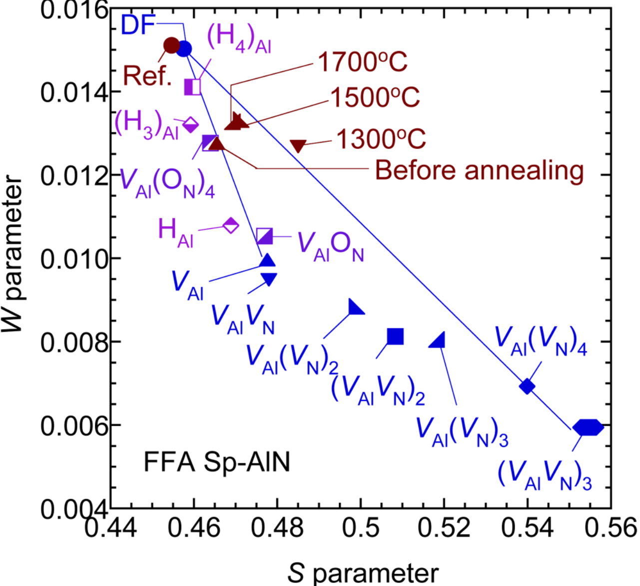


**FIG. 4.** $S$–$W$ relationships for FFA Sp-AlN measured at $E = 4$ keV using a coincidence system (brown). ($S$,$W$) value for MOVPE-AlN (ref.) is also shown. Annealing temperatures (1300–1700 °C) are shown in the figure. Calculated ($S$,$W$) values (blue) for positron annihilation in defect-free (DF) AlN, $V_{Al}$, $V_{Al}(V_N)_n$ (n = 1–4), $(V_{Al}V_N)_n$ (n = 1, 2), $V_{Al}(O_N)_m$ (m = 1,4), and $(H_n)_{Al}$ (n = 1, 3, and 4) are also shown.


Published under license by AIP Publishing.

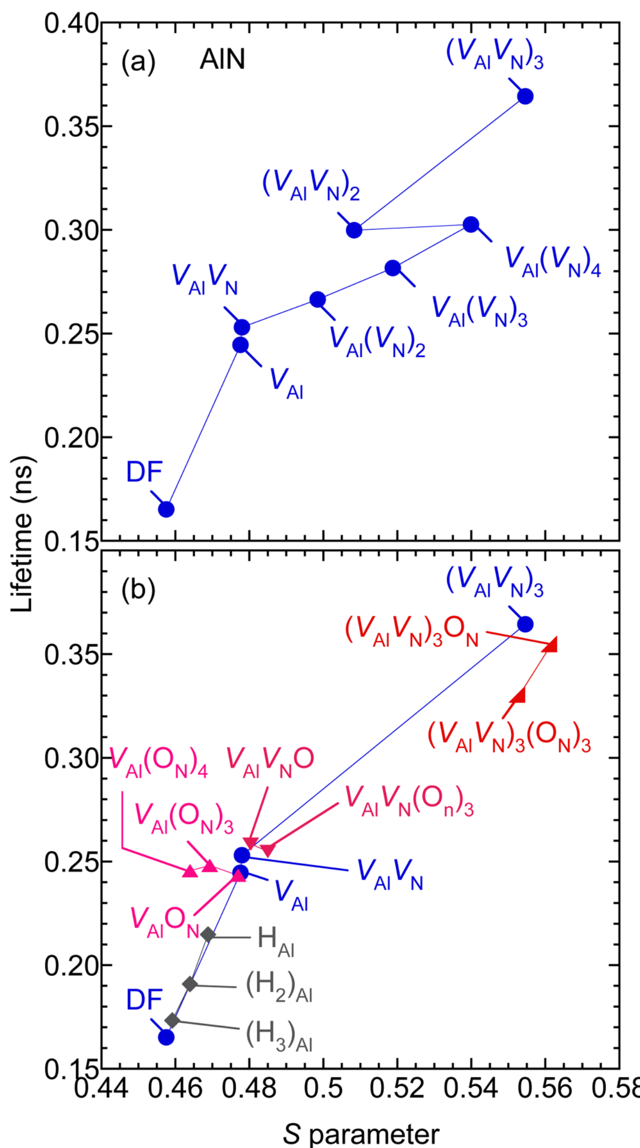


**FIG. 5.** Relationships between calculated $S$ values and lifetimes of positrons for (a) typical intrinsic vacancies and (b) their complexes between vacancies and oxygen or hydrogen atoms.

The lifetime spectra of positrons for the FFA Sp-AlN films were also measured at $E = 4$ keV, and they were decomposed into two components. The mean positron lifetime $\tau_m$ was calculated by the equation $\tau_m = \Sigma\tau_i I_i$ (i = 1,2), and they are shown in Fig. 2(c). Figure 6 shows the values of $\tau_1$, $\tau_2$, and $I_2$ as a function of annealing temperature. For the as-deposited sample, the second lifetime was determined to be $\tau_2 = 0.2403 \pm 0.001$ ns [Fig. 6(b)]. This lifetime was close to the calculated lifetime of $V_{Al}$ or $V_{Al}(O_N)_n$ (Fig. 5). Because the value of $I_2$ was $82 \pm 2\%$, the second component was the major annihilation mode of positrons in this sample. In Fig. 4,

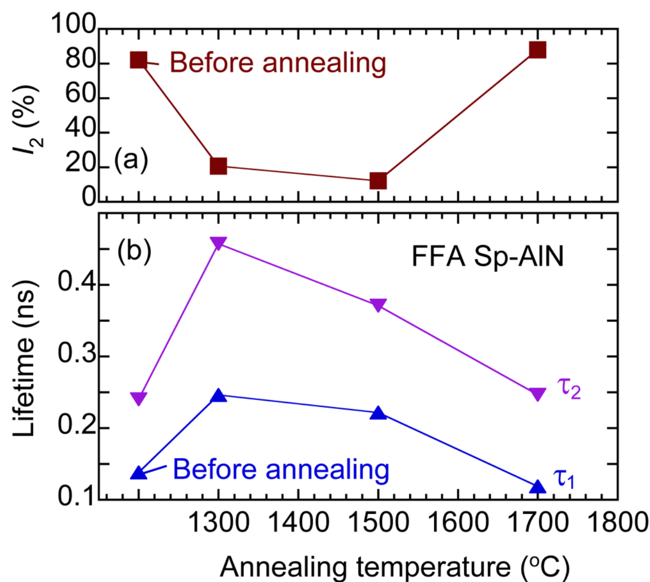


**FIG. 6.** (a) Annealing behaviors of relative intensity corresponding to second annihilation mode ($I_2$) and (b) lifetimes of positrons ($\tau_1$ and $\tau_2$) measured at $E = 4$ keV for FFA Sp-AlN.

the $(S,W)$ value for this sample was close to that for $V_{Al}(O_N)_4$ and far from the value of $V_{Al}$. Thus, the major defect species in the as-deposited AlN film was determined to be $V_{Al}(O_N)_n$. The formation energy of $V_{Al}$ decreased as the number of oxygen atoms coupled with $V_{Al}$ increased.[44] Because of the high oxygen concentration in the FFA Sp-AlN films ($[O] = 6 \times 10^{20}$ cm$^{-3}$), $V_{Al}(O_N)_n$ must have been the dominant defects. A similar conclusion for bulk PVT-AlN was also reported by Mäki *et al.*[27] In their report, the lifetime of positrons trapped by $V_{Al}$ was reported to be 0.210 ns, which is shorter than the value of $\tau_2$ (0.240 ns) for the as-deposited sample. When bulk semiconductors with high melting points are grown by the PVT method, impurities in the sample are expected to be oxygen, Si, carbon, and hydrogen, where these materials are incorporated during the growth process, either as a part of the source materials in the crucible or reactor parts.[18,45] As shown in Fig. 5, the trapping of hydrogen by $V_{Al}$ decreased the positron lifetime. Thus, the difference in the measured positron lifetimes for $V_{Al}$-related defects [such as $V_{Al}$ and $V_{Al}(O_N)_n$] could be the effect of hydrogen on their lifetimes.

For the as-deposited sample, on the basis of the trapping model, the value of $\tau_b$ was calculated to be 0.212 ns, which was longer than the calculated lifetime for defect-free AlN. This suggests that the value of $\tau_1$ increased due to the effect of the trapping of positrons by the vacancy-type defects. The value of [H] in the as-deposited sample was high ($[H] = 3 \times 10^{19}$ cm$^{-3}$). As discussed above, the incorporation of hydrogen into $V_{Al}$ decreases the lifetime of positrons trapped by such defects. Thus, the first component would be attributed to the annihilation of positrons trapped by $V_{Al}$-H complexes. The high-temperature annealing at 1700 °C caused out-diffusion of hydrogen, and [H]


Published under license by AIP Publishing.

became $\leq 6 \times 10^{16}$ cm$^{-3}$. Because vacancies with the concentration of $10^{16}$–$10^{17}$ cm$^{-3}$ are a detectable range of positron annihilation,[19] the $\tau_1$ value for the sample annealed at 1700 °C would be still influenced by hydrogen.

Another possibility which decreases the positron lifetime is shallow positron traps. Mäki *et al.*[27] reported that negatively charged non-open volume defects acted as shallow hydrogenic traps for positron in PVT-AlN at room temperature. The presence of shallow traps suppresses the trapping of positrons by vacancy-type defects. An origin of shallow traps in AlN is not clear but candidates are negatively charged impurities, micro-clusters of impurities, etc. In general, the $(S,W)$ values for such shallow traps, however, are close to the value for the annihilation of positrons in the delocalized state.[43] Thus, an incorporation of the annihilation of positrons trapped by such traps shifts the $(S,W)$ value toward the defect-free value along the line connecting the values of the

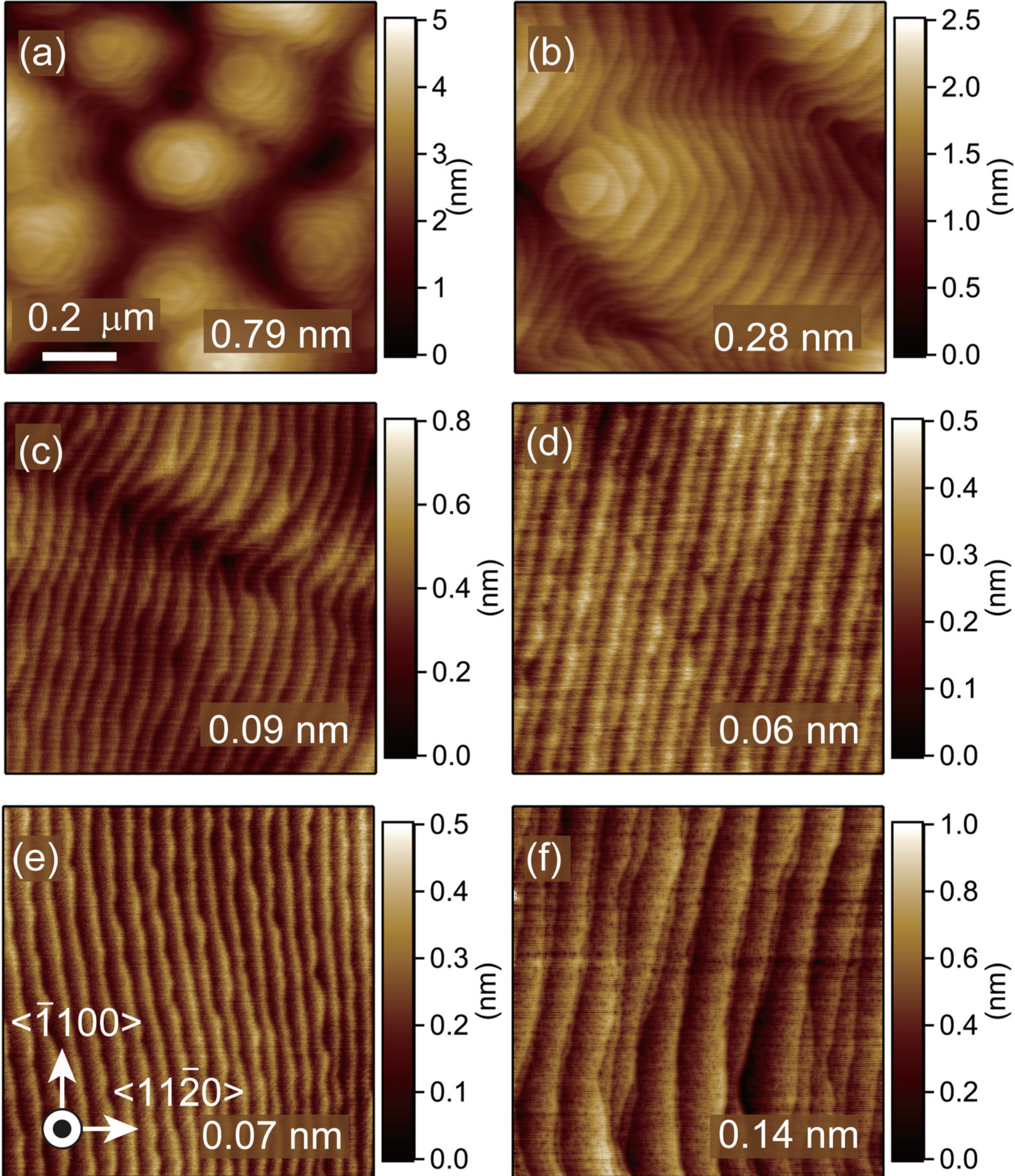


**FIG. 7.** AFM images of MOVPE-AlN grown on FFA Sp-AlN at (a) 1100 °C, (b) 1150 °C, (c) 1200 °C, (d) 1300 °C, and (e) 1340 °C. For AlN grown at 1300 °C, image obtained after annealing at 1700 °C is also shown as (f). Scanning area was 1 × 1 $\mu$m$^2$. RMS roughness of sample surfaces is shown in the figure.


Published under license by AIP Publishing.

defect-free state and the vacancy-type defects. Therefore, even under the influence of the shallow traps, the identification of major defect species using the $S$–$W$ plot is possible if the major defect spices are vacancy-type defects.

As shown in Fig. 6, both $\tau_1$ and $\tau_2$ increased after annealing at 1300 °C. Because the $\tau_1$ value was close to $\tau_2$ for the sample before annealing, the first annihilation mode can be attributed to the trapping of positrons by $V_{Al}(O_N)_n$. The value of $\tau_2$ was determined to be 0.46 ± 0.01 ns. Because this lifetime was longer than the lifetime of positrons trapped by $(V_{Al}V_N)_3$ (Fig. 5), the size of the vacancy-type defects introduced by 1300 °C annealing was larger than such defects. As shown in Fig. 4, the $(S,W)$ values for large defects tended to be located in the lower right of the $S$–$W$ plot. For the sample after annealing at 1300 °C, the $(S,W)$ value shifted toward the right-hand side, suggesting an introduction of large vacancy clusters. Thus, the same conclusion was reached both from the $S$–$W$ plot and the lifetime measurements. Although the introduction of vacancy clusters was observed after 1300 °C annealing, because the $I_2$ value was 21 ± 1%, the trapping of positrons by $V_{Al}(O_N)_n$ was still the major annihilation mode.

After annealing at 1500 °C, the values of $\tau_2$ and $I_2$ started to decrease, which was due to the dissociation of vacancy clusters and a decrease in their concentration. The $(S,W)$ tended to return back to the position for the as-deposited sample. For the sample annealed at 1700 °C, the second component was the major annihilation mode ($\tau_2$ = 0.247 ± 0.001 ns and $I_2$ = 88 ± 1%), and this mode was again identified as the trapping of positrons by $V_{Al}(O_N)_n$. Comparing between the $(S,W)$ values for the as-deposited sample and the one annealed at 1700 °C, the $(S,W)$ value shifted to the right-hand side after annealing, suggesting a decrease in the effect of the trapping of positrons by $V_{Al}(O_N)_n$.

### D. Defect characterization of MOVPE-AlN

Figure 7 shows AFM images of the MOVPE-AlN films with different growth temperatures (1100–1340 °C). As shown in Fig. 7(a), 3D island growth was the major growth mechanism at a growth temperature of 1100 and 1150 °C. Note that there were no dislocation cores at the centers of the 3D islands, as shown in Figs. 7(a) and 7(b). Therefore, it can be confirmed that these 3D islands were not originated by screw-dislocation-induced spiral growth. These surface morphologies can be observed from the AlN epilayers on low-screw-dislocation templates grown with high surface supersaturation conditions.[46] As the temperature increased, the RMS roughness decreased, and a monolayer was observed above 1300 °C. After annealing at 1700 °C for the sample grown at 1300 °C, monolayer steps observed before annealing became bilayer steps. The RMS roughness of the sample surface is shown in the figure, and its annealing behavior is shown in Fig. 8(a). Figure 8(b) shows the FWHM of the (0002) and $(10\bar{1}2)$-plane diffraction peaks. There was no large change in the FWHM values before and after annealing at 1700 °C. The FWHM values of the diffraction peaks were close to those reported for the samples prepared by similar growth conditions.[10] The value of screw and edge TDDs estimated from the FWHMs of (0002) and $(10\bar{1}2)$-plane diffraction peaks were around $1 \times 10^6$ and $2 \times 10^8$ cm$^{-2}$, respectively.

Figure 8(c) shows the annealing behavior of $S$ measured at $E$ = 10 keV for the MOVPE-AlN films. The value of $S$ increased as the growth temperature increased (1100–1300 °C) but decreased at 1340 °C annealing. For the sample grown at 1300 °C, the $S$ value decreased after post-growth annealing at 1700 °C. Figure 9 shows the $S$–$W$ relationships for the MOVPE-AlN films. The $(S,W)$ value for the sample after annealing at 1700 °C is also shown. In the figure, a line connects the $(S,W)$ values for DF and $V_{Al}$, and another one connects the values for DF and $V_{Al}(V_N)_4$ (see Fig. 4). With the increasing growth temperature (1100–1300 °C), the $(S,W)$ value shifted toward the lower right side, which can be associated with the effect of positron annihilation in vacancy clusters, such as $V_{Al}(V_N)_4$ or $(V_{Al}V_N)_n$. For the sample with a growth temperature at 1340 °C, however, the $(S,W)$ value tended to approach that of $V_{Al}(O_N)_4$. For the reactor used in the present work, oxygen incorporation in the sample started above the growth temperature at 1300 °C, where the source of oxygen was the quartz tubes used in the reactor. Thus, the observed decrease in the value of $S$ for this sample (Fig. 8) was not due to the decrease in the defect concentration but to the

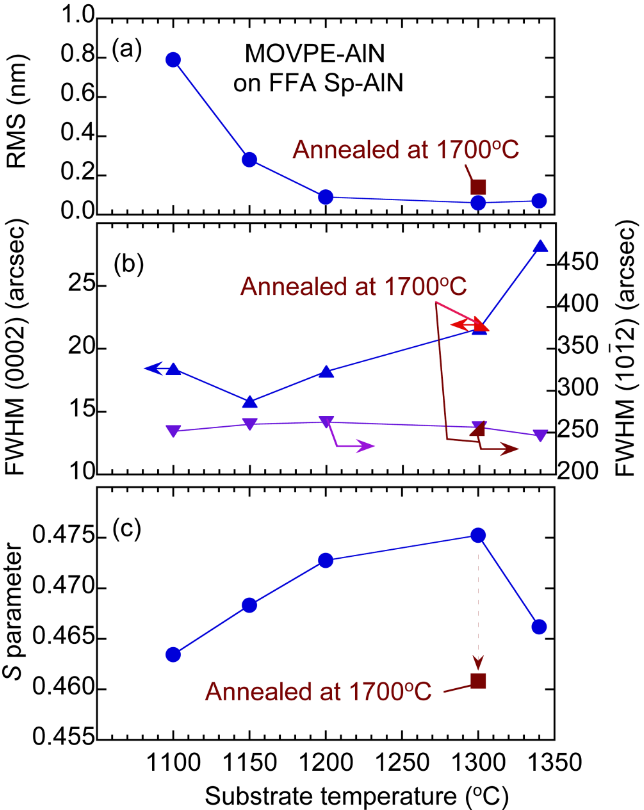


**FIG. 8.** Annealing behaviors of (a) RMS roughness of sample surface, (b) FWHM of (0002) and $(10\bar{1}2)$-plane x-ray diffraction peaks, and (c) $S$ values measured at $E$ = 8 keV for MOVPE-AlN on FFA Sp-AlN with different growth temperatures (1100–1340 °C). Results for AlN grown at 1300 °C after annealing at 1700 °C are also shown.



Published under license by AIP Publishing.

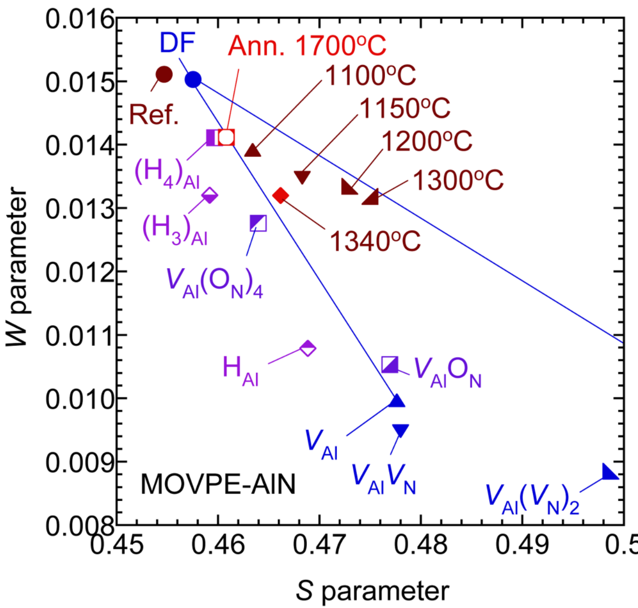


FIG. 9. *S*–*W* relationships for MOVPE-AlN grown on FFA Sp-AlN measured at $E = 8$ keV using coincidence system (brown). Growth temperature (1100–1340 °C) of the sample is shown in the figure. Line in figure connects (*S*,*W*) values for DF and $V_{Al}$, and another connects (*S*,*W*) values for DF and $V_{Al}(V_N)_4$ (see Fig. 4). Calculated (*S*,*W*) values are also shown (blue and violet).

introduction of complexes between vacancies and oxygen atoms. For the sample annealed at 1700 °C, the (*S*,*W*) value was located on the line that connects the (*S*,*W*) values for the sample before the annealing and the reference sample. Thus, the annealing treatment at 1700 °C was effective for decreasing the vacancy-type defects introduced at the high growth temperature.

## IV. SUMMARY

We used monoenergetic positron beams to study vacancy-type defects in AlN films deposited by using RF sputtering and MOVPE. For the Sp-AlN films before annealing treatment, the major defect species was identified as vacancy–oxygen complexes such as $V_{Al}(O_N)_n$. The introduction of such defects was attributed to the high oxygen concentration in the FFA Sp-AlN films ($[O] = 6 \times 10^{20}$ cm$^{-3}$) and the suppression of the formation energy of $V_{Al}$ by coupling with oxygen. After annealing at 1300 °C, vacancy clusters, such as $V_{Al}(V_N)_4$ and $(V_{Al}V_N)_3$, were introduced but their concentrations decreased above 1500 °C annealing. The major defect species in the FFA Sp-AlN films, however, were still vacancy–oxygen complexes even at 1700 °C annealing. For the MOVPE-AlN films, although the surface roughness improved, the concentration of vacancy clusters increased as the growth temperature increased (1100–1300 °C). The concentration of such defects decreased after post-growth annealing at 1700 °C. The present work shows that a positron annihilation is a powerful tool for characterizing native defects in AlN. The knowledge obtained about defect species and their annealing behaviors will be useful for optimizing growth parameters and post-growth treatments of AlN films.

## ACKNOWLEDGMENTS

This work was supported by JSPS KAKENHI (Grant Nos. 16H06415, 16H06418, 16H06424, 16H06427, and 19K15025). A part of this work was also supported by the MEXT "Program for research and development of next-generation semiconductor to realize energy-saving society" and "Program for Building Regional Innovation Ecosystems."

## DATA AVAILABILITY

The data that support the findings of this study are available within this article.

## REFERENCES

[1]H. Hirayama, J. Appl. Phys. **97**, 091101 (2005).
[2]M. Kneissl and J. Rass, "III-nitride ultraviolet emitters," in *Springer Series in Materials Science* (Springer, Berlin, 2016).
[3]Y. Nagasawa and A. Hirano, Appl. Sci. **8**, 1264 (2018).
[4]M. Kneissl, T. Y. Seong, J. Han, and H. Amano, Nat. Photonics **13**, 233 (2019).
[5]J. Zhang, X. Hu, A. Lunev, J. Deng, Y. Bilenko, T. M. Katona, M. S. Shur, R. Gaska, and M. A. Khan, Jpn. J. Appl. Phys. **44**, 7250 (2005).
[6]J. Bai, M. Dudley, W. H. Sun, H. M. Wang, and M. A. Khan, Appl. Phys. Lett. **88**, 051903 (2006).
[7]S. Inoue, T. Naoki, T. Kinoshita, T. Obata, and H. Yanagi, Appl. Phys. Lett. **106**, 131104 (2015).
[8]H. Miyake, G. Nishio, S. Suzuki, K. Hiramatsu, H. Fukuyama, J. Kaur, and N. Kuwano, Appl. Phys. Express **9**, 025501 (2016).
[9]H. Fukuyama, H. Miyake, G. Nishio, S. Suzuki, and K. Hiramatsu, Jpn. J. Appl. Phys. **55**, 05FL02 (2016).
[10]H. Miyake, C. H. Lin, K. Tokoro, and K. Hiramatsu, J. Cryst. Growth **456**, 155 (2016).
[11]C. G. Van de Walle and J. Neugebauer, J. Appl. Phys. **95**, 3851 (2004).
[12]K. Uesugi, Y. Hayashi, K. Shojiki, and H. Miyake, Appl. Phys. Express **12**, 065501 (2019).
[13]K. B. Nam, J. Li, M. L. Nakarmi, J. Y. Lin, and H. X. Jiang, Appl. Phys. Lett. **82**, 1694 (2003).
[14]T. Onuma, K. Hazu, A. Uedono, T. Sota, and S. F. Chichibu, Appl. Phys. Lett. **96**, 061906 (2010).
[15]S. F. Chichibu, T. Onuma, K. Hazu, and A. Uedono, Appl. Phys. Lett. **97**, 201904 (2010).
[16]R. Collazo, J. Xie, B. E. Gaddy, Z. Bryan, R. Kirste, M. Hoffmann, R. Dalmau, B. Moody, Y. Kumagai, T. Nagashima, Y. Kubota, T. Kinoshita, A. Koukitu, D. L. Irving, and Z. Sitar, Appl. Phys. Lett. **100**, 191914 (2012).
[17]J. Glaab, J. Haefke, J. Ruschel, M. Brendel, J. Rass, T. Kolbe, A. Knauer, M. Weyers, S. Einfeldt, M. Guttmann, C. Kuhn, J. Enslin, T. Wernicke, and M. Kneissl, J. Appl. Phys. **123**, 104502 (2018).
[18]S. F. Chichibu, K. Kojima, K. Hazu, Y. Ishikawa, K. Furusawa, S. Mita, R. Collazo, Z. Sitar, and A. Uedono, Appl. Phys. Lett. **115**, 151903 (2019).
[19]R. Krause-Rehberg and H. S. Leipner, *Positron Annihilation in Semiconductors, Solid-State Sciences* (Springer-Verlag, Berlin, 1999), Vol. 127.
[20]F. Tuomisto and I. Makkonen, Rev. Mod. Phys. **85**, 1583 (2013).
[21]K. Saarinen, T. Laine, S. Kuisma, J. Nissilä, P. Hautojärvi, L. Dobrzynski, J. M. Baranowski, K. Pakula, R. Stepniewski, M. Wojdak, A. Wysmolek, T. Suski, M. Leszczynski, I. Grzegory, and S. Porowski, Phys. Rev. Lett. **79**, 3030 (1997).
[22]K. Saarinen, T. Suski, I. Grzegory, and D. C. Look, Phys. Rev. B **64**, 233201 (2001).


Published under license by AIP Publishing.

[23]A. Uedono, S. F. Chichibu, Z. Q. Chen, M. Sumiya, R. Suzuki, T. Ohdaira, T. Mikado, T. Mukai, and S. Nakamura, J. Appl. Phys. **90**, 181 (2001).
[24]J. Slotte, F. Tuomisto, K. Saarinen, C. G. Moe, S. Keller, and S. P. DenBaars, Appl. Phys. Lett. **90**, 151908 (2007).
[25]F. Tuomisto, J. M. Mäki, T. Yu Chemekova, Y. N. Makarov, O. V. Avdeev, E. N. Mokhov, A. S. Segal, M. G. Ramm, S. Davis, G. Huminic, H. Helava, M. Bickermann, and B. M. Epelbaum, J. Cryst. Growth **310**, 3998 (2008).
[26]A. Uedono, S. Ishibashi, S. Keller, C. Moe, P. Cantu, T. M. Katona, D. S. Kamber, Y. Wu, E. Letts, S. A. Newman, S. Nakamura, J. S. Speck, U. K. Mishra, S. P. DenBaars, T. Onuma, and S. F. Chichibu, J. Appl. Phys. **105**, 054501 (2009).
[27]J. M. Mäki, I. Makkonen, F. Tuomisto, A. Karjalainen, S. Suihkonen, J. Raisanen, T. Y. Chemekova, and Y. N. Makarov, Phys. Rev. B **84**, 081204(R) (2011).
[28]R. Ye, J. D. Liu, H. J. Zhang, and B. J. Ye, Appl. Phys. Lett. **115**, 262401 (2019).
[29]S. Xiao, R. Suzuki, H. Miyake, S. Harada, and T. Ujihara, J. Cryst. Growth **502**, 41 (2018).
[30]A. Uedono, M. Imanishi, M. Imade, M. Yoshimura, S. Ishibashi, M. Sumiya, and Y. Mori, J. Cryst. Growth **475**, 261 (2017).
[31]A. van Veen, H. Schut, M. Clement, J. M. M. de Nijs, A. Kruseman, and M. R. IJpma, Appl. Surf. Sci. **85**, 216 (1995).
[32]P. Sperr, W. Egger, G. Kögel, G. Dollinger, C. Hugenschmidt, R. Repper, and C. Piochacz, Appl. Surf. Sci. **255**, 35 (2008).
[33]C. Hugenschmidt, C. Piochacz, M. Reiner, and K. Schreckenbach, New J. Phys. **14**, 055027 (2012).
[34]P. Kirkegaard, M. Eldrup, O. E. Mogensen, and N. J. Pedersen, Comput. Phys. Commun. **23**, 307 (1981).
[35]S. Ishibashi, T. Tamura, S. Tanaka, M. Kohyama, and K. Terakura, Phys. Rev. B **76**, 153310 (2007).
[36]S. Ishibashi and A. Uedono, J. Phys. Conf. Ser. **505**, 012010 (2014).
[37]P. E. Blöchl, Phys. Rev. B **50**, 17953 (1994).
[38]G. Kresse and D. Joubert, Phys. Rev. B **59**, 1758 (1999).
[39]J. P. Perdew, K. Burke, and M. Ernzerhof, Phys. Rev. Lett. **77**, 3865 (1996).
[40]S. Ishibashi, A. Uedono, H. Kino, T. Miyake, and K. Terakura, J. Phys. Condens. Matter **31**, 475401 (2019).
[41]E. Boroński and R. M. Nieminen, Phys. Rev. B **34**, 3820 (1986).
[42]A. Uedono, Y. Tsukada, Y. Mikawa, T. Mochizuki, H. Fujisawa, H. Ikeda, K. Kurihara, K. Fujito, S. Terada, S. Ishibashi, and S. F. Chichibu, J. Cryst. Growth **448**, 117 (2016).
[43]A. Uedono, S. Takashima, M. Edo, K. Ueno, H. Matsuyama, H. Kudo, H. Naramoto, and S. Ishibashi, Phys. Status Solidi B **252**, 2794 (2015).
[44]Q. Yan, A. Janotti, M. Scheffler, and C. G. Van de Walle, Appl. Phys. Lett. **105**, 111104 (2014).
[45]R. Kirste and Z. Sitar, in *Semiconductors and Their Modern Devices*, edited by B. Gil (Oxford University Press, 2013).
[46]I. Bryan, Z. Bryan, S. Mita, A. Rice, J. Tweedie, R. Collazo, and Z. Sitar, J. Cryst. Growth **438**, 81 (2016).


Published under license by AIP Publishing.